Tensile Strain Switched Ferromagnetism in Layered NbS_2 and $NbSe_2$

Yungang Zhou,[†,‡] Zhiguo Wang,[†] Ping Yang,[‡] Xiaotao Zu,[†,*] Li Yang,[†] Xin Sun,[‡] and Fei Gao[‡,*]

[†]Department of Applied Physics, University of Electronic Science and Technology of China, Chengdu, 610054, People's Republic of China and
[‡]Pacific Northwest National Laboratory, P.O. Box 999, Richland, Washington 99352, United States

ABSTRACT Developing approaches to effectively induce and control the magnetic states is critical to the use of magnetic nanostructures in quantum information devices but is still challenging. Here we have demonstrated, by employing the density functional theory calculations, the existence of infinite magnetic sheets with structural integrity and magnetic homogeneity. Examination of a series of transition metal dichalcogenides shows that the biaxial tensile strained NbS_2 and $NbSe_2$ structures can be magnetized with a ferromagnetic character due to the competitive effects of through-bond interaction and through-space interaction. The estimated Curie temperatures (387 and 542 K under the 10% strain for NbS_2 and $NbSe_2$ structures, respectively) suggest that the unique ferromagnetic character can be achieved above room temperature. The self-exchange of population between 4d orbitals of the Nb atom that leads to exchange splitting is the mechanism behind the transition of the spin moment. The induced magnetic moments can be significantly enhanced by the tensile strain, even giving rise to a half-metallic character with a strong spin polarization around the Fermi level. Given the recent progress in achieving the desired strain on two-dimensional nanostructures, such as graphene and a BN layer, in a controlled way, we believe that our calculated results are suitable for experimental verification and implementation, opening a new path to explore the spintronics in pristine two-dimensional nanostructures.

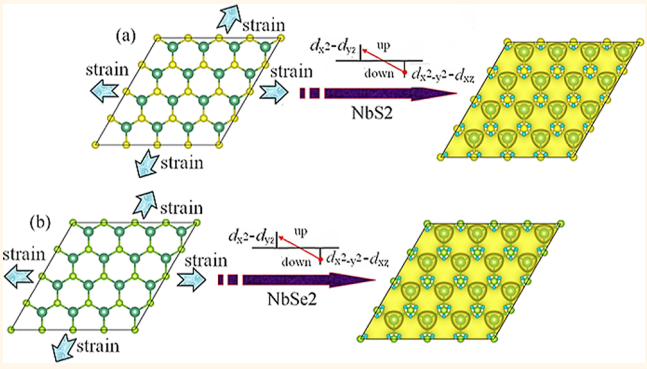

KEYWORDS: NbS_2 · $NbSe_2$ · biaxial strain · magnetism · density functional theory

Two-dimensional nanosheet crystals have been the subject of intensive research in the fabrication of nanoscale devices.[1−7] Among these, the transition metal dichalcogenides (TMDs) of MX_2 type (M = Mo, W, Nb, Re, Ti, Ta, *etc.* and X = S, Se, Te), which have a honeycomb structure with a thickness down to three atomic layers, exhibit a large variety of electronic phases such as metals,[8−10] semiconductors,[11−16] and superconductors[17] depending on the coordination and oxidation state of the metal atoms. Recently, different strategies have been proposed to synthesize these materials on a stable nanometric scale, such as hydrothermal processes,[18] mechanical activation at high temperature,[19] or shape transformation from one-dimensional (1D) nanorods to two-dimensional (2D) nanosheet crystals.[20] Exciting examples include the following: Coleman *et al.* successfully synthesized layered compounds, such as MoS_2, WS_2, $MoSe_2$, $MoTe_2$, $TaSe_2$, $NbSe_2$, and $NiTe_2$, and demonstrated that these 2D TMDs can be efficiently dispersed in common solvents as individual flakes or formed into films;[21] thin films of MoS_2, $TaSe_2$, WS_2, $MoSe_2$, and $NbSe_2$ have also been fabricated by large-scale exfoliation of inorganic layered compounds in aqueous surfactant solutions;[22] using a new wet chemistry approach, high-quality 2D nanosheet crystals of MoS_2 and WS_2 were obtained by Altavilla *et al.*[23] The possible applications of these materials, such as transistors,[24] photoemitting devices,[25,26] photovoltaics,[27] catalysis,[28] hydrogen storage,[29] lubricants,[30] and Li-ion batteries,[31] have been proposed and investigated. However, novel magnetic properties have not yet been found in these pristine TMDs, and most TMDs are nonmagnetic. A number of experimental and theoretical results have shown that the embedment of transition metal (TM) atoms can induce magnetism in nonmagnetic nanomaterials.[32−41]

* Address correspondence to fei.gao@pnnl.gov, xtzu@uestc.edu.cn.

Received for review July 17, 2012 and accepted October 11, 2012.

Published online October 11, 2012
10.1021/nn303198w

© 2012 American Chemical Society

The scientific issue is whether TMDs with so many TM atoms can be magnetized. If indeed intriguing magnetic properties exist, possible magnetic applications, especially above room temperature, must be pursued. In order to unlock the valuable properties, theoretical studies mainly focus on the edge structure, defect, and doping in these 2D materials, which may play a certain role in the introduction of magnetic behaviors. For example, Li *et al*. indicated that zigzag MoS_2 nanoribbons exhibit ferromagnetic and metallic behavior irrespective of the ribbon width and thickness.[42] With defects and doping in MoS_2 nanoribbons, the nonmagnetic and magnetic nanoribbons can be tuned depending on where the foreign atoms are adsorbed and what kind of vacancy defect is created.[43] For WS_2 nanoribbons, the zigzag edges of W(0%S)−S(50%), W(0%S)−S(100%), W(100%S)−S(100%), and W(50%S)−S(100%) types can also turn out to be magnetic.[44] However, in bringing TMDs up to the level of practical applications, we encountered the follow fundamental difficulties: (1) until now few methods are proposed for the successful fabrication of TMD nanoribbons, and the mass production of TMD nanoribbon-based devices is beyond the capability of current technology; (2) the induced magnetic properties depend strongly on the type of defects and position of doping, while the precise control of defects and doping on TMDs in the nanoscale remains challenging.

As an alternative, one promising route to manipulate magnetic properties is elastic strain engineering.[45,46] Although the appearance of ferromagnetic (FM) coupling in FeCu alloy because of the increase of the lattice constant has been proposed by recent experimental studies,[47] large elastic strain rarely exists in bulk materials since they are easily relaxed by dislocation plasticity or fracture. In contrast, the plasticity and fracture in nanostructures are greatly delayed, which allow for a much larger dynamical range of applying elastic strain reversibly. For example, the measured breaking strength is as high as 13% for a graphene monolayer, while that of bulk graphite seldom reaches 0.1%.[48,49] Considering the interplay between the mechanical properties and magnetic behavior, it was predicted that the tensile strain along the zigzag direction can significantly enhance magnetic moments and the stability of FM coupling of the graphene with a topological line defect.[50] With similar structures, such as half-fluorinated BN and GaN layers, an intriguing antiferromagnetism (AFM) → FM coupling transition can also occur by applying strain, even giving rise to a half-metallic character when the sheets are under a compression of 6%.[51] These studies suggest that strain can be potentially used as an effective pathway to induce and engineer the magnetic properties of nanomaterials. Thus, in light of these previous studies, a systematical understanding of strain effect on magnetic behavior of these TMDs would be highly desirable.

TABLE 1. Calculated Structural Parameters (lattice constant, a_{NbS2}; S−S bond length, d_{S-S}; Nb−S bond length, d_{Nb-S}) in the NbS_2 Structure and Structural Parameters (lattice constant, a_{NbSe2}; Se−Se bond length, d_{Se-Se}; Nb−Se bond length, d_{Nb-Se}) in the $NbSe_2$ Structure

	strain										
	0%	1%	2%	3%	4%	5%	6%	7%	8%	9%	10%
a_{NbS2} (Å)	3.35	3.39	3.42	3.46	3.49	3.52	3.56	3.59	3.62	3.66	3.69
d_{S-S} (Å)	3.14	3.11	3.09	3.07	3.05	3.04	3.02	3.00	2.99	2.97	2.96
d_{Nb-S} (Å)	2.49	2.50	2.51	2.52	2.53	2.54	2.55	2.56	2.57	2.58	2.59
a_{NbSe2} (Å)	3.48	3.51	3.55	3.58	3.62	3.66	3.69	3.73	3.76	3.80	3.83
d_{Se-Se} (Å)	3.37	3.34	3.32	3.30	3.28	3.26	3.25	3.23	3.21	3.20	3.18
d_{Nb-Se} (Å)	2.62	2.63	2.64	2.65	2.66	2.67	2.68	2.69	2.70	2.71	2.73

The present studies are prompted by the recent experiments where the desired strain can be achieved on 2D nanostructures, such as graphene and a BN layer in a controlled way,[52−54] and thus, our calculated results are suitable for experimental verification and implementation. In this paper, we explore the electronic properties in a series of TMDs using density functional theory calculations and demonstrate that only NbX_2 (X = S, Se) structures can be magnetized by simply applying a tensile strain. The self-exchange of population between the 4d orbitals of the Nb atom is the mechanism behind the transition of spin moment in the calculations. Two crucial characteristics are found for the induced magnetism: (1) the induced spin magnetizations in NbX_2 structures exhibit a substantial FM ordering character through long-rang magnetic coupling; (2) when the strain reaches 10%, NbX_2 structures yield a half-metal character, associated with the strong spin polarization around the Fermi level. Thus, the above-mentioned findings provide a new pathway to explore NbX_2-based spintronics. In contrast to previous studies, our results exhibit the following advantages over the existing ones: (1) it is not necessary to substitutionally or by adsorption dope Nb and X atoms in NbX_2 structures by foreign atoms such as Fe, Co, Ni, and Mn, around which the magnetism may appear; (2) it is not necessary to introduce Nb and X vacancies in NbX_2 structures, near which the magnetism may be induced; (3) it is not necessary to cut two-dimensional NbX_2 layers into finite systems with zigzag edges (like one-dimensional ribbons or zero-dimensional nanoflakes), at which the magnetism may occur. Although these methods can be achieved experimentally, until now the precise control of doping and forming vacancies on TMDs at the nanoscale is still challenging, and also the magnetism in zigzag edges can be easily quenched during assembly.

RESULTS AND DISCUSSION

Our systematic study begins with the geometric details of NbS_2 and $NbSe_2$ listed in Table 1. Under zero

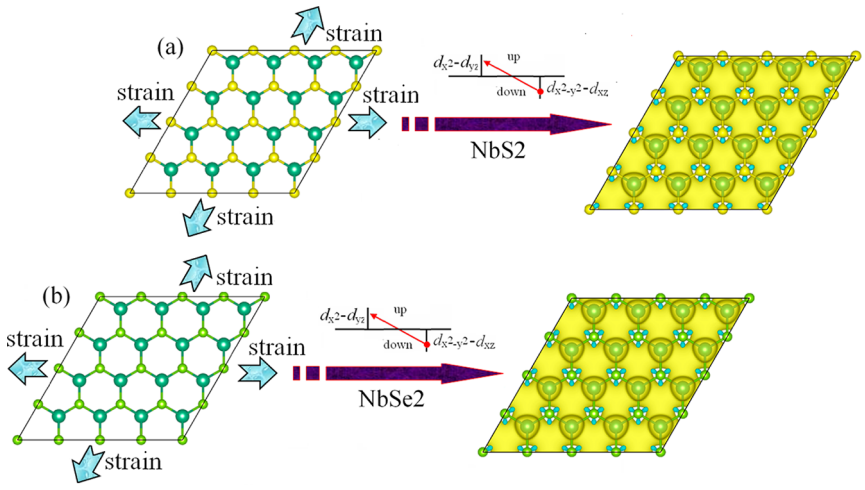

Figure 1. Schematic illustration of the biaxial strain-induced magnetism for (a) NbS_2 and (b) $NbSe_2$ structures. The insets show the electron transfer between different orbitals due to the biaxial strain. The small yellow, small blue, and large blue balls represent S, Se, and Nb atoms, respectively, in the geometric structures. The yellow and blue isosurfaces correspond to the spin-up and spin-down components, respectively, in the spatial spin density distributions.

strain, the computed lattice parameters of NbS_2 (a_{NbS2} = 3.35, d_{S-S} = 3.14 and d_{Nb-S} = 2.49 Å) and $NbSe_2$ (a_{NbSe2} = 3.48, d_{Se-Se} = 3.37 and d_{Nb-Se} = 2.62 Å) are in good agreement with previous results.[8−10] Upon applying a biaxial tensile strain (the biaxial tensile strain here is defined as $\varepsilon = \Delta c/c_0$, where lattice constants of the unstrained and strained supercell are equal to c_0 and $c = \Delta c + c_0$, respectively) on these materials, a_{NbS2} and a_{NbSe2} increase. Because of in-plane biaxial tensile strain, a deformation in the perpendicular direction is likely to occur, which is reminiscent of deformation in a nanotube by a uniaxial strain along the nanotube in our previous studies,[55,56] and thus the distances of S−S and Se−Se (denoted as d_{S-S} and d_{Se-Se}) become small. The decrease of d_{S-S} and d_{Se-Se} retards the increase of d_{Nb-S} and d_{Nb-Se}. The increase of bonding lengths was found to be only 4% for both NbS_2 and $NbSe_2$ structures at a 10% tensile strain, as compared to the 10% increase of bonding lengths in graphene and the BN layer for the same tensile strain. Consequently, the relatively small change in the bonding lengths in NbS_2 and $NbSe_2$ implies a relatively large range of elastic limits where the structural breakage or phase transition would not occur, thus, a possibility to well control the electronic and magnetic properties of these structures compared with graphene and a BN layer.

Theoretical calculations based on density functional theory have revealed that NbS_2 and $NbSe_2$ are metallic[8−10] and may play important roles in device applications. Previous studies show that such half-filled metal states with local states near the Fermi level are closely associated with magnetism.[33,57] Indeed, our calculations demonstrate that, when the tensile strain is applied to these structures, spin-polarized states are observed, as depicted in Figure 1. For example, the unstrained NbS_2 and $NbSe_2$ are not spontaneously magnetized, while the 5% tensile strain can induce about 0.50 and 0.61 μ_B (per unit cell) in NbS_2 and $NbSe_2$, respectively. Thus, the magnetic behavior in NbX_2 structures is transferred from nonmagnetism to magnetism when the tensile strain is applied, while the magnetic behavior is transferred from low magnetism to high magnetism in VX_2 structures.[45] The interplay between the mechanical properties and their magnetic behaviors is represented in Figure 2a and b. Here the magnetic moments of S and Nb atoms in the NbS_2 structure are denoted M_S and M_{Nb}, respectively, and the magnetic moments of Se and Nb atoms in the $NbSe_2$ structure are denoted M_{Se} and M_{Nb}, respectively. The M_S in the NbS_2 structure begins to increase when the strain is 3%, which is defined as a critical tensile strain. The increase of magnetic moment exhibits a nearly linear relationship with the tensile strain. In the $NbSe_2$ structure, the basic behavior of M_{Se} is the same as that found for M_S, but the critical tensile strain appears at 2% due to the difference in ionic radii between S and Se atoms. It should be noted that the magnetic moments in both structures are spin-down and very small. When the tensile strain increases to 10%, the M_S and M_{Se} increase only 0.018 and 0.028 μ_B, respectively. In contrast, the M_{Nb} in both structures is spin-up and rapidly increases with the tensile strain. The increase of magnetic moment exhibits a parabolic behavior with the tensile strain. Yet, when the tensile strain increases to 10%, the M_{Nb} in NbS_2 and $NbSe_2$ structures can possess 0.52 and 0.67 μ_B, respectively. These results clearly suggest that Nb atoms mainly dominate the spin polarizations, while the contribution from S and Se atoms can be almost negligible. In order to establish these unique magnetic properties experimentally, the possible structure breakage or phase transition with increasing strain must be better understood. In this regard, Figure 2c exhibits the variation of total energies with tensile strain. The monotonically

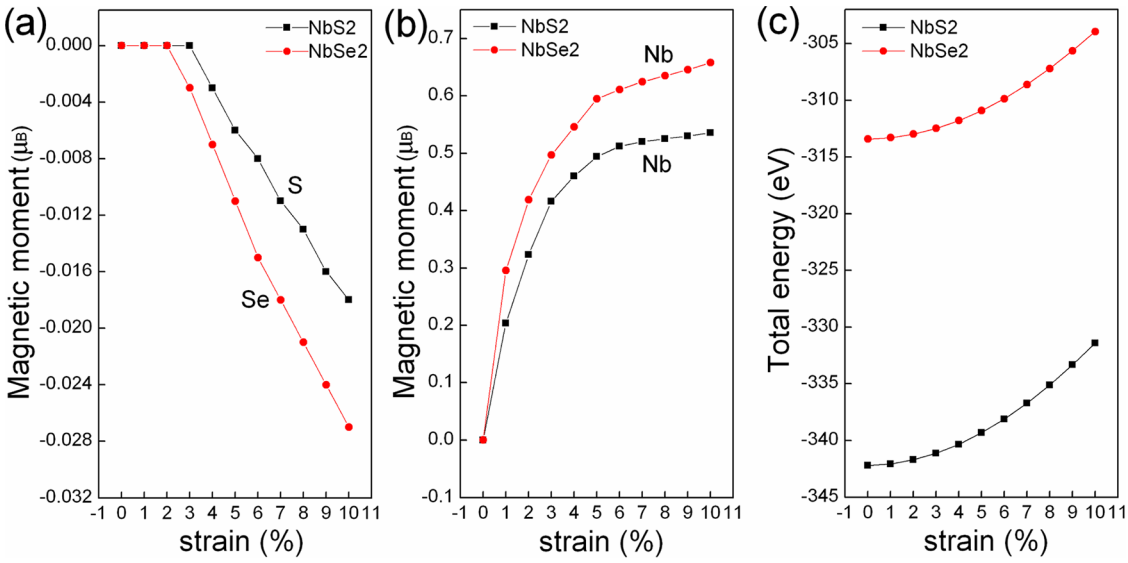

Figure 2. Strain dependence of magnetic moment (a) per S and Se atoms in NbS_2 and $NbSe_2$ structures, respectively, (b) per Nb atom in NbS_2 and $NbSe_2$ structures, and (c) of the total energy variation in both structures.

increased tendency elucidates a large elastic range because of the unique geometry structure mentioned above, in which the structure breakage or phase transition will not occur, and may have two important applications: (1) it is anticipated that the large elastic range would display substantial magnetism, which is expected for establishing the nanomagnets, serving as an excellent probe tip in magnetic atomic force microscopy, or utilizing as magnetic attraction drug delivery in pharmaceutical systems in the living body; (2) the large elastic range provides a large space to achieve the reverse process where the applied tensile or compressive strains in the NbX_2 lattice can modify the spin state of the system, which is significant for practical electromechanical nanodevice applications. For example, the ultrathin NbX_2 structures can be designed for the logic states assigned as "0" with small spin state or "1" with large spin state, achieving a desired spin switch.

These interesting changes of the spin polarization with the tensile strain can be attributed to the particular interactions between the Nb and X atoms in NbX_2 structures. An isolated Nb atom has a $4d^{4\uparrow}5s^{1\uparrow}$ configuration with a spin exchange splitting of 2.3 eV. A number of experimental and theoretical results have suggested that such TM atom embedded in a nonmagnetic nanomaterial can induce magnetism due to the partially filled d character of the TM atoms.[32−41] Interestingly, the layered NbX_2 (X = S and Se) structure consisting of so many Nb atoms here has been proved to possess a particular d character[8−10] and thus is expected to contain a range of magnetic behaviors. However, the Nb atoms in NbX_2 structures are sandwiched between two layers of X atoms, forming a strong ligand field due to the Nb−X covalent bond and thus quenching the magnetism of the Nb atoms. Examination of the hybridization states shows that the covalent bonds are mainly ascribed to the Nb 4d and S 3p (or Se 4p) orbitals. In fact, the quenching of the magnetic moment of TM atoms due to the covalent interaction is in agreement with previous studies.[8−10] Thus, the reduction of covalent interactions between Nb−X bonds becomes the effective means for the magnetic induction. When the NbX_2 structure is under a finite tensile strain, the bonding energy of the Nb in the NbX_2 structure decreases with increasing biaxial strain, as expected. For example, when the strain is increased from 0% to 10%, the calculated binding energies decrease from 15.2 to 10.3 eV for the Nb in the NbS_2 structure and from 14.6 to 9.8 eV in the $NbSe_2$ structures. In contrast, we find no magnetic induction in the compressed NbX_2 structure due to the increase in the Nb−X covalent interaction. Thus, we consider the tensile strain for studying the magnetic behaviors of only the layered NbX_2 structure. As can be seen from Figure 3, the electronic properties of NbX_2 with respect to the tensile strain confirm the above speculation. Near the Fermi level, the S 3p states in the NbS_2 structure (or Se 4p in the $NbSe_2$ structure) are somewhat decreased with an increase in strain, and thus, they no longer take part in the hybridized interaction with Nb atoms. As a consequence, the exchange splitting of Nb 4d states may be unlocked due to the reduction of the hybridization with S 3p states (or Se 4p states). However, the change of S 3p states near the Fermi level is very small and almost negligible, and the most important effect comes from the hybridized states, with energies ranging from −4.5 to −0.3 eV, which further supports the above discussion. It has been proven that the hybridized character at these energy regions is responsible for the spin polarization near the Fermi level and can translate into a

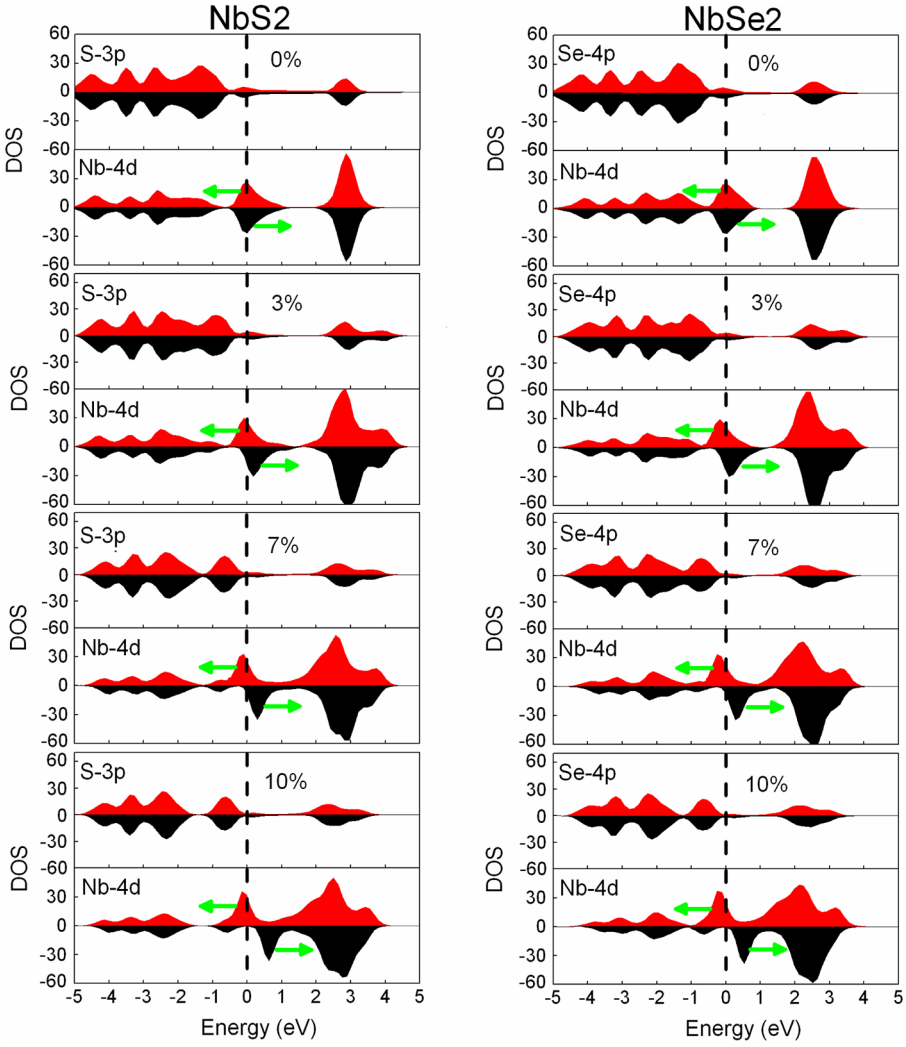

Figure 3. Spin-polarized partial density of states (DOS) of NbS_2 and $NbSe_2$ structures under 0%, 3%, 7%, and 10% biaxial strain. The red and black regions represent the spin-up and spin-down components, respectively, where the Fermi level is indicated by the dashed line. The blue arrows indicate the spin splitting near the Fermi level.

perturbation for the polarized atom.[35] On the basis of this conclusion, the exchange splitting of the Nb atoms in the NbX_2 structure appears to be much smaller than the typical value obtained for an isolated Nb atom. With the increase of tensile strain, the hybridized states at these energy regions remarkably decrease, which decreases the perturbations and in turn enhances the splitting effect. Thus, the reduced hybridized states in low-energy regions can be viewed as a main effect for unlocking the exchange splitting of the Nb atoms and leading to the unique spin moment of NbX_2.

In order to further understand the splitting effect by the tensile strain, the evolutions of spin-polarized band structures under 0%, 3%, 7%, and 10% tensile strain are shown in Figure 4. All band structures exhibit a qualitatively similar behavior that indicates the less populated spin-down orbitals and the more populated spin-up orbitals. The spin degeneracy is thus broken. From detailed examination, the spin-up and spin-down electronic states near the Fermi level are dominated by the mixed Nb $d_{x^2}-d_{yz}$ orbitals and mixed Nb $d_{x^2-y^2}-d_{xz}$ orbitals, respectively, suggesting that the interesting splitting effect can be attributed to the self-exchanging of Nb 4d electrons (*i.e.*, Nb $d_{x^2-y^2}-d_{xz} \rightarrow$ Nb $d_{x^2}-d_{yz}$ transfer), as suggested in Figure 1. Considering the possible electron transfer between Nb and X atoms due to the change of bonding lengths, we also calculated the variation of total charge in X and Nb atoms shown in Figure 5b. Even at 10% tensile strain, each Nb loses only about 0.11 |e| for both structures, and each S in the NbS_2 structure and each Se in the $NbSe_2$ structure gain only about 0.05 and 0.08 |e|, respectively, implying a relatively small charge transfer between Nb and X atoms. Therefore, the self-exchange of population between 4d orbitals of the Nb atom can be viewed as an important mechanism for the exchange splittings, which induces spin moment transition. However, in VX_2 structures, the relative transfer of electrons between V and X atoms plays an important role in the transition of the spin moment.[45] The calculated

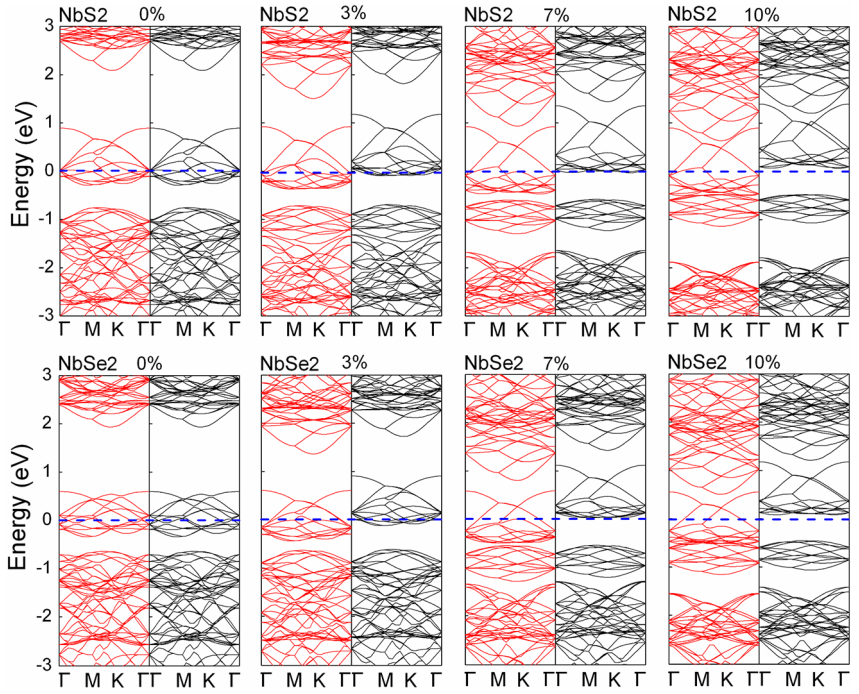

Figure 4. Spin-polarized band structures of NbS_2 and $NbSe_2$ under 0%, 3%, 7%, and 10% biaxial strain. The red and black lines represent the spin-up and spin-down components, respectively, where the Fermi level is indicated by the dashed line.

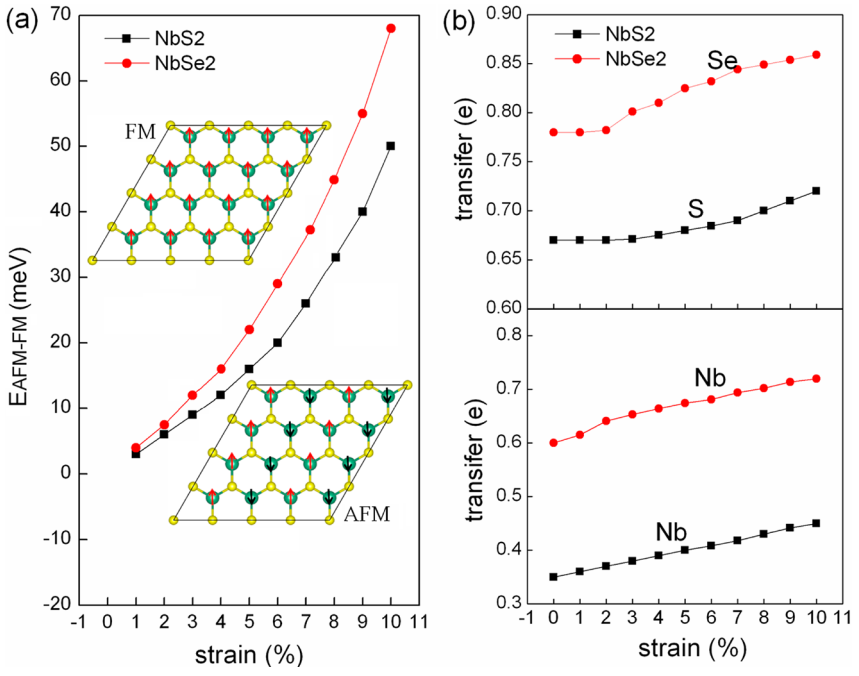

Figure 5. Strain dependence of (a) the energy difference per unit cell between FM and AFM coupling and (b) the electron transfer of S, Se, and Nb atoms in NbS_2 and $NbSe_2$ structures. The insets in (a) give the schematic illustrations of FM and AFM couplings.

exchange splittings are about 0, 0.22, 0.30, and 0.38 eV under 0%, 3%, 7%, and 10% strains, respectively, in the NbS_2 structure and 0, 0.24, 0.36, and 0.42 eV under 0%, 3%, 7%, and 10% strains, respectively, in the $NbSe_2$ structure. The tendency is in agreement with the finding of net moments (per unit cell) of 0, 0.41, 0.51, and 0.53 μ_B for 0%, 3%, 7%, and 10% strains, respectively, in the NbS_2 structure and 0, 0.50, 0.63, and 0.68 μ_B for 0%, 3%, 7% and 10% strains, respectively, in the $NbSe_2$ structure. In order to achieve a confirmed conclusion, we have performed a series of calculations to investigate the magnetic behavior of other 2D TMDs such as MoS_2, WS_2, $MoSe_2$, and WSe_2. It is of interest to find that no magnetism is observed in

these materials under tensile strain. Since as described above the unusual magnetic behaviors in NbS_2 and $NbSe_2$ structures are associated with not only the increased bond lengths by strain but also the particular metallic character, the TMDs such as MoS_2, WS_2, $MoSe_2$, and WSe_2 are nonmagnetic due to the presence of certain band gaps. Comparing the two different effects, we can appreciate the partially filled d character of the Nb atoms that induces the metallic character in NbX_2. In fact, the difference in strain-induced magnetic behaviors depending on the metallic and semiconducting characters of the host structure has been proposed in Ni-substituted graphene and nanotubes.[33,35]

In Figure 4, the energy level of these spin-up and spin-down states near the Fermi level as a function of the applied tensile strain determines the observed physical features of the 2D NbX_2 structures. These special changes of electronic states suggest interesting transitions occurred under tensile strain (*i.e.*, nonmagnetic metal → magnetic metal → half-metal transitions). The layered NbX_2 with a strong Nb−X bond is a nonmagnetic metal from the onset, in agreement with Kuc *et al.*'s prediction.[8−10] With a finite strain (from 0% to 10%), a splitting effect was detected, which changes NbX_2 to a magnetic metal. When a strain of up to 10% is applied, a typical half-metal character occurs, in which one level in the spin-up channel crosses the Fermi level and the corresponding level in the spin-down channel does not. Thus, the interesting magnetism with a collective character found here under tensile strain enables the 2D nanolayers to be spin-filtering layers. To visualize the spin distribution on the NbX_2 structures, we also impose spin density in Figure 1. It can be clearly seen that the charge density is rather spherical around the Nb atoms, while the X atoms have a very small magnetic moment. Conventionally, the induced magnetism is often located on adsorbed atoms or near vacant sites. However, for a doped system, one of the crucial issues for its applications in spintronic devices is whether the local spin moments induced by defect states can lead to a collective magnetism, which is an essential requirement for any spintronic application. Unfortunately, this critical issue, as well as its implications, was often overlooked in the previous studies of the doping-induced magnetism of nanostructures. Thus, the finding of a substantial collective character with a long-range magnetic coupling by tensile strain here offers a new avenue to facilitate the design of controllable and tunable spin devices.

Considering the practical applications in nanoelectronics, the spin ordering of Nb atoms is more important.[58−62] Therefore, we have explored the spin-ordering dependence on strain in NbX_2 structures. Two stable magnetic structures (*i.e.*, FM and AFM coupling structures) are considered. The energy difference, $\Delta E = E_{AFM} - E_{FM}$, per unit cell as a function of tensile strain is presented in Figure 5a. As spin polarization is not observed in unstrained NbX_2 structures, we investigated the spin ordering from 1% tensile strain. For a relatively small tensile strain, such as 1%, the FM coupling is favored over the AFM coupling (*i.e.*, $\Delta E > 0$), while the energy difference is only 2 meV. In this case, the FM coupling is not very stable, and it is impractical to use such a structure for device applications, such as nanoscale magnets and spin transport, at room temperature. Fortunately, the tensile strain on NbX_2 enhances not only the value of the magnetic moment mentioned above but also the stability of the magnetic state. In Figure 5a, it is of great interest to find that the FM spin coupling is always more stable than the AFM spin coupling. The energy difference increases with the strain, which displays a very similar behavior for both structures. When the tensile strain is increased up to 10%, the energy difference can reach 50 and 68 meV for NbS_2 and $NbSe_2$ structures, nearly 25- and 34-fold increases compared to that of the 1% strain. As a matter of fact, for strains above 10%, the energy difference between FM and AFM coupling in NbS_2 and $NbSe_2$ structures will further increase with the strain. However, if a large strain is applied, structural breakage or phase transition may occur, leading to an energy difference of zero. According to the Heisenberg model,[63] $H = -J\sum_i \sigma_i \sigma_{i+1}$, where J is the exchange coupling parameter and σ_i is the net spin induced by ith vacancy, the ΔE in these structures can be deduced as $\Delta E = 2J|\sigma_i|^2$.[45] The calculated exchange coupling parameters are about 92 and 78 meV under the 10% strain, compared to about zero under 1% strain, for NbS_2 and $NbSe_2$ structures, respectively, indicating an appreciable magnetic coupling. Thus, upon the increase of tensile strain, the stability of magnetic exchange coupling (*i.e.*, FM spin ordering) can be enhanced. In order to further probe whether this coupling is appreciable for the applications of NbX_2 above room temperatures, we also estimate the Curie temperature, T_C, according the Heisenberg model. The magnetic energy difference, ΔE, can be described using the mean-field value of T_C with $k_B T_C = (2/3)\Delta E$.[64] The calculated values under 10% strain are about 387 and 542 K for NbS_2 and $NbSe_2$ structures, respectively, which are higher than room temperature. This result suggests that the ferromagnetic NbS_2 and $NbSe_2$ structures can be utilized above room temperature. In fact, the stress-induced Curie temperature enhancement has been experimentally proposed in $Fe_{64}Ni_{36}$ Invar alloy because of the increase of Fe−Fe interatomic distances, which reinforces ferromagnetic interactions.[65] Notably, here the enhanced Curie temperature of NbX_2 structures is due to the increased Nb−Nb interatomic distances.

For magnetic 2D compounds, the coupling mechanism (*i.e.*, through-bond coupling interaction and through-space coupling interaction) has been successfully

proposed by Ma *et al.*[51] According to the currently calculated results, the mechanism also well holds for the layered NbX_2 structures. It was noted that for through-bond coupling interaction, an atom with up-spin (down-spin) can induce a down-spin (up-spin) on adjacent atoms directly bonded to it. For NbX_2 systems here, the magnetic relation between M_{Nb} and M_X can be presented as "... $M_{Nb} \rightarrow -M_X \rightarrow M_{Nb}$ ...". Thus, for this coupling interaction, all Nb atoms in NbX_2 structures are FM coupling and can retain the same spin alignment, as shown in Figure 5a. As a matter of fact, the interaction of through-bond coupling has also been previously reported to explain the room-temperature FM character in cation-vacancy-induced magnetism in GaN.[64] On the other hand, for a through-space coupling interaction, an atom with an up-spin (down-spin) density induces a down-spin (up-spin) density on the nearest-neighboring atom directly, without a mediation atom. For NbX_2 systems here, the magnetic relation of M_{Nb} can be represented as "... $M_{Nb} \rightarrow -M_{Nb}$ ...". In this coupling interaction, the AFM coupling appears in the Nb atoms, as shown in Figure 5a. Thus, on the basis of the above descriptions, the stable magnetic structures can be explained as a competitive effect of through-bond interaction and through-space interaction. When through-bond interaction is stronger than through-space interaction, NbX_2 exhibits FM coupling; otherwise it exhibits AFM coupling. Since the valence electrons of Nb 4d states that contribute to the magnetism are relatively localized in the NbX_2 structures, as illustrated in Figure 3, they have relatively small spatial extension but a strong Nb−X covalent interaction, which leads to the directly through-space interaction being smaller than the through-bond interaction, and thus the FM coupling becomes more stable than the AFM coupling. As a matter of fact, a similar phenomenon also has been found in VX_2.[45] However, due to the difference in the binding interaction between NbX_2 and VX_2 structures, NbX_2 structures might have a unique Curie temperature for practical applications. In contrast, in half-fluorinated graphene and BN layers, the 2p states of magnetic atoms are more delocalized and have much larger spatial extension that promotes direct through-space interaction and results in a more stable AFM coupling than the FM coupling.[51] The reliability of this mechanism is also well reflected by the variations in energy between FM and AFM with tensile strain. With the increase of tensile strain, the bond lengths between Nb and X atoms increase, which results in the reduction of both through-bond interactions and through-space interactions. However, for the d state coupling in this work,[45] opposite of the p state coupling,[51] the reduction of through-space interaction is larger than that of through-bond interaction, effectively explaining the increase in the energy difference between the AFM and FM coupling with the tensile strain, as shown in Figure 5a. On the basis of these results, it is expected that the energy difference between AFM and FM can reach a high value when the tensile strain is large enough. Furthermore, from our examination the maximum elastic strain that NbX_2 can take is over 50% (*i.e.*, no structural breakage or phase transition was observed under the large strain), which provides a very effective solution for stabilizing the magnetic state and allows the 2D NbX_2 structures to be practically used in room-temperature conditions.

CONCLUSIONS

In summary, spin-polarized density functional theory calculations have been conducted to study the electronic structures and magnetic properties of layered NbS_2 and $NbSe_2$ under a biaxial strain. Under the applied biaxial tensile strain, the layered NbS_2 and $NbSe_2$ structures can be evinced to establish the magnetic behaviors with a ferromagnetic character, which is attributed to the competitive effects of through-bond and through-space interactions. The self-exchange of the population between 4d orbitals of the Nb atom leads to exchange splitting, which is an important mechanism behind the transition of the spin moment. The induced spin magnetizations align parallel and exhibit a substantial collective character, which is a crucial issue for the spin-circuit application that is often overlooked in previous studies on doping-induced magnetism of nanostructures. Furthermore, the tensile strain on NbS_2 and $NbSe_2$ structures enhances not only the value of the magnetic moment but also the stability of the ferromagnetic coupling. The estimated Curie temperatures suggest that the ferromagnetic NbS_2 and $NbSe_2$ structures are suitable for spin applications above room temperature. Given the recent progress in achieving the desired strain on 2D nanostructures, such as graphene and BN layers in a controlled way,[52−54] we believe that our calculated results are suitable for experimental verification and implementation.

COMPUTATIONAL METHOD

The first-principles periodic calculations based on density functional theory are performed using the Vienna *ab initio* simulation package (VASP). Within the generalized gradient approximation (GGA), we considered Perdew−Burke−Ernzerhof exchange and correlation functionals. The electronic wave functions were expanded using a plane-wave basis set with a cutoff energy of 520 eV. In our calculations, the structures of 4×4 supercells of NbS_2 and $NbSe_2$ are used with a vacuum space of 15 Å between two layers to avoid interactions between them. Pseudopotentials with $3s^2 3p^4$, $4s^2 4p^4$, and $4d^4 5s^1$ valence electron configurations, respectively, for S, Se, and Nb atoms are used. The stresses of different magnitudes are applied along the biaxial directions by changing the cell parameters, after which

the structures are relaxed. For the optimizations of these structures, Brillouin zone integration was performed using a $8 \times 8 \times 1$ *k*-point grid, and for electronic structural optimization a $12 \times 12 \times 1$ *k*-point grid was used. All the calculations were carried out with spin-polarization, and the atomic positions of the structure were relaxed until all the force components were smaller than 0.01 eV/Å. In order to conveniently compare with previous work based on GGA (neglecting the GGA+U method),[8−10] we in this work also employ the GGA method.

Conflict of Interest: The authors declare no competing financial interest.

Acknowledgment. This study was financially supported by the Division of Materials Sciences and Engineering, Office of Basic Energy Sciences, U.S. Department of Energy, under Contract DE-AC05-76RL01830. The authors also wish to thank the Molecular Science Computing Facility in the Environmental Molecular Sciences Laboratory at the Pacific Northwest National Laboratory for a grant of computer time. This study was also supported financially by the National Natural Science Foundation of China (61178018).

REFERENCES AND NOTES

1. Hwang, H.; Joo, P.; Kang, M. S.; Ahn, G.; Han, J. T.; Kim, B.-S.; Cho, J. H. Highly Tunable Charge Transport in Layer-by-Layer Assembled Graphene Transistors. *ACS Nano* **2012**, *6*, 2432–2440.
2. Zhang, Y.; Ye, J.; Matsuhashi, Y.; Iwasa, Y. Ambipolar MoS_2 Thin Flake Transistors. *Nano Lett.* **2012**, *12*, 1136–1140.
3. Radisavljevic, B.; Whitwick, M. B.; Kis, A. Integrated Circuits and Logic Operations Based on Single-Layer MoS_2. *ACS Nano* **2011**, *5*, 9934–9938.
4. Kim, T.; Kirn, H.; Kwon, S. W.; Kim, Y.; Park, W. K.; Yoon, D. H.; Jang, A. R.; Shin, H. S.; Suh, K. S.; Yang, W. S. Large-Scale Graphene Micropatterns *via* Self-Assembly-Mediated Process for Flexible Device Application. *Nano Lett.* **2012**, *12*, 743–748.
5. Li, H.; Yin, Z. Y.; He, Q. Y.; Huang, X.; Lu, G.; Fam, D. W. H.; Tok, A. I. Y.; Zhang, Q.; Zhang, H. Fabrication of Single- and Multilayer MoS_2 Film-Based Field-Effect Transistors for Sensing NO at Room Temperature. *Small* **2012**, *8*, 63–67.
6. Yin, Z.; Li, H.; Li, H.; Jiang, L.; Shi, Y.; Sun, Y.; Lu, G.; Zhang, Q.; Chen, X.; Zhang, H. Single-Layer MoS_2 Phototransistors. *ACS Nano* **2012**, *6*, 74–80.
7. Sire, C.; Ardiaca, F.; Lepilliet, S.; Seo, J.-W. T.; Hersam, M. C.; Dambrine, G.; Happy, H.; Derycke, V. Flexible Gigahertz Transistors Derived from Solution-Based Single-Layer Graphene. *Nano Lett.* **2012**, *12*, 1184–1188.
8. Kuc, A.; Zibouche, N.; Heine, T. Influence of Quantum Confinement on the Electronic Structure of the Transition Metal Sulfide TS_2. *Phys. Rev. B* **2011**, *83*, 245213.
9. Ivanovskaya, V. V.; Zobelli, A.; Gloter, A.; Brun, N.; Serin, V.; Colliex, C. *Ab Initio* Study of Bilateral Doping within the MoS(2)-NbS(2) System. *Phys. Rev. B* **2008**, *78*, 134104.
10. Lebegue, S.; Eriksson, O. Electronic Structure of Two-dimensional Crystals from *Ab Initio* Theory. *Phys. Rev. B* **2009**, *79*, 115409.
11. Topsakal, M.; Ciraci, S. Effects of Static Charging and Exfoliation of Layered Crystals. *Phys. Rev. B* **2012**, *85*, 045121.
12. Ramasubramaniam, A.; Naveh, D.; Towe, E. Tunable Band Gaps in Bilayer Transition-Metal Dichalcogenides. *Phys. Rev. B* **2011**, *84*, 205325.
13. Ma, Y. D.; Dai, Y.; Guo, M.; Niu, C. W.; Huang, B. B. Graphene Adhesion on MoS_2 Monolayer: An *Ab Initio* Study. *Nanoscale* **2011**, *3*, 3883–3887.
14. Ma, Y. D.; Dai, Y.; Guo, M.; Niu, C. W.; Lu, J. B.; Huang, B. B. Electronic and Magnetic Properties of Perfect, Vacancy-Doped, and Nonmetal Adsorbed MoSe(2), MoTe(2) and WS(2) Monolayers. *Phys. Chem. Chem. Phys.* **2011**, *13*, 15546–15553.
15. Yun, W. S.; Han, S. W.; Hong, S. C.; Kim, I. G.; Lee, J. D. Thickness and Strain Effects on Electronic Structures of Transition Metal Dichalcogenides: 2H-MX_2 Semiconductors (M = Mo, W; X = S, Se, Te). *Phys. Rev. B* **2012**, *85*, 033305.
16. Zhu, Z. Y.; Cheng, Y. C.; Schwingenschlogl, U. Giant Spin-Orbit-Induced Spin Splitting in Two-Dimensional Transition-Metal Dichalcogenide Semiconductors. *Phys. Rev. B* **2011**, *84*, 153402.
17. Friend, R. H.; Yoffe, A. D. Electronic Properties of Intercalation Complexes of the Transition Metal Dichalcogenides. *Adv. Phys.* **1987**, *36*, 1–94.
18. Peng, Y.; Meng, Z.; Zhong, C.; Lu, J.; Yu, W.; Jia, Y.; Qian, Y. Hydrothermal Synthesis and Characterization of Single-Molecular-Layer MoS_2 and $MoSe_2$. *Chem. Lett.* **2001**, *8*, 772–773.
19. Wu, Z. Z.; Wang, D. Z.; Zan, X. Q.; Sun, A. K. Synthesis of WS(2) Nanosheets by A Novel Mechanical Activation Method. *Mater. Lett.* **2010**, *64*, 856–858.
20. Seo, J. W.; Jun, Y. W.; Park, S. W.; Nah, H.; Moon, T.; Park, B.; Kim, J. G.; Kim, Y. J.; Cheon, J. Two-Dimensional Nanosheet Crystals. *Angew. Chem., Int. Ed.* **2007**, *46*, 8828–8831.
21. Coleman, J. N.; Lotya, M.; O'Neill, A.; Bergin, S. D.; King, P. J.; Khan, U.; Young, K.; Gaucher, A.; De, S.; Smith, R. J.; *et al.* Two-Dimensional Nanosheets Produced by Liquid Exfoliation of Layered Materials. *Science* **2011**, *331*, 568–571.
22. Smith, R. J.; King, P. J.; Lotya, M.; Wirtz, C.; Khan, U.; De, S.; O'Neill, A.; Duesberg, G. S.; Grunlan, J. C.; Moriarty, G.; *et al.* Large-Scale Exfoliation of Inorganic Layered Compounds in Aqueous Surfactant Solutions. *Adv. Mater.* **2011**, *23*, 3944–3948.
23. Altavilla, C.; Sarno, M.; Ciambelli, P. A Novel Wet Chemistry Approach for the Synthesis of Hybrid 2D Free-Floating Single or Multilayer Nanosheets of MS_2@oleylamine (M=Mo, W). *Chem. Mater.* **2011**, *23*, 3879–3885.
24. Radisavljevic, B.; Radenovic, A.; Brivio, J.; Giacometti, V.; Kis, A. Single-Layer MoS_2 Transistors. *Nat. Nanotechnol.* **2011**, *6*, 147–150.
25. Aharon, E.; Albo, A.; Kalina, M.; Frey, G. L. Stable Blue Emission from a Polyfluorene/Layered-Compound Guest/Host Nanocomposite. *Adv. Funct. Mater.* **2006**, *16*, 980–986.
26. Splendiani, A.; Sun, L.; Zhang, Y.; Li, T.; Kim, J.; Chim, C.-Y.; Galli, G.; Wang, F. Emerging Photoluminescence in Monolayer MoS_2. *Nano Lett.* **2010**, *10*, 1271–1275.
27. Thomalla, M.; Tributsch, H. Photosensitization of Nanostructured TiO_2 with WS_2 Quantum Sheets. *J. Phys. Chem. B* **2006**, *110*, 12167–12171.
28. Hu, K. H.; Hu, X. G.; Xu, Y. F.; Pan, X. Z. Reaction Kinetics Mechanisms and Catalysis. *React. Kinet. Mech. Catal.* **2010**, *100*, 153–163.
29. Seayad, A. M.; Antonelli, D. M. Recent Advances in Hydrogen Storage in Metal-Containing Inorganic Nanostructures and Related Materials. *Adv. Mater.* **2004**, *16*, 765–777.
30. Mosleh, M.; Atnafu, N. D.; Belk, J. H.; Nobles, O. M. Modification of Sheet Metal Forming Fluids with Dispersed Nanoparticles for Improved Lubrication. *Wear* **2009**, *267*, 1220–1225.
31. Xiao, J.; Wang, X. J.; Yang, X. Q.; Xun, S. D.; Liu, G.; Koech, P. K.; Liu, J.; Lemmon, J. P. Electrochemically Induced High Capacity Displacement Reaction of PEO/MoS(2)/Graphene Nanocomposites with Lithium. *Adv. Funct. Mater.* **2011**, *21*, 2840–2846.
32. Ataca, C.; Ciraci, S. Functionalization of Single-Layer MoS_2 Honeycomb Structures. *J. Phys. Chem. C* **2011**, *115*, 13303–13311.
33. Santos, E. J. G.; Ayuela, A.; Sánchez-Portal, D. Strain-Tunable Spin Moment in Ni-Doped Graphene. *J. Phys. Chem. C* **2011**, *116*, 1174–1178.
34. Huang, B.; Yu, J. J.; Wei, S. H. Strain Control of Magnetism in Graphene Decorated by Transition-Metal Atoms. *Phys. Rev. B* **2011**, *84*, 075415.
35. Santos, E. J. G.; Ayuela, A.; Fagan, S. B.; Mendes, J.; Azevedo, D. L.; Souza, A. G.; Sanchez-Portal, D. Switching on Magnetism in Ni-Doped Graphene: Density Functional Calculations. *Phys. Rev. B* **2008**, *78*, 195420.
36. Li, Y. F.; Zhou, Z.; Jin, P.; Chen, Y. S.; Zhang, S. B. B.; Chen, Z. F. Achieving Ferromagnetism in Single-Crystalline ZnS Wurtzite Nanowires *via* Chromium Doping. *J. Phys. Chem. C* **2010**, *114*, 12099–12103.

37. Zhou, J.; Wang, L.; Qin, R.; Zheng, J. X.; Mei, W. N.; Dowben, P. A.; Nagase, S.; Gao, Z. X.; Lu, J. Structure and Electronic and Transport Properties of Transition Metal Intercalated Graphene and Graphene-Hexagonal-Boron-Nitride Bilayer. *J. Phys. Chem. C* **2011**, *115*, 25273–25280.
38. Durgun, E.; Akman, N.; Ciraci, S. Functionalization of Silicon Nanowires with Transition Metal Atoms. *Phys. Rev. B* **2008**, *78*, 195116.
39. Ataca, C.; Cahangirov, S.; Durgun, E.; Jang, Y. R.; Ciraci, S. Structural, Electronic, and Magnetic Properties of 3*d* Transition Metal Monatomic Chains: First-Principles Calculations. *Phys. Rev. B* **2008**, *77*, 214413.
40. Sevincli, H.; Topsakal, M.; Durgun, E.; Ciraci, S. Electronic and Magnetic Properties of 3d Transition-Metal Atom Adsorbed Graphene and Graphene Nanoribbons. *Phys. Rev. B* **2008**, *77*, 195434.
41. Yildirim, T.; Iniguez, J.; Ciraci, S. Molecular and Dissociative Adsorption of Multiple Hydrogen Molecules on Transition Metal Decorated C-60. *Phys. Rev. B* **2005**, *72*, 153403.
42. Li, Y. F.; Zhou, Z.; Zhang, S. B.; Chen, Z. F. MoS(2) Nanoribbons: High Stability and Unusual Electronic and Magnetic Properties. *J. Am. Chem. Soc.* **2008**, *130*, 16739–16744.
43. Ataca, C.; Sahin, H.; Akturk, E.; Ciraci, S. Mechanical and Electronic Properties of MoS(2) Nanoribbons and Their Defects. *J. Phys. Chem. C* **2011**, *115*, 3934–3941.
44. Wang, Z.; Zhao, K.; Li, H.; Liu, Z.; Shi, Z.; Lu, J.; Suenaga, K.; Joung, S.-K.; Okazaki, T.; Jin, Z.; *et al*. Ultra-Narrow WS_2 Nanoribbons Encapsulated in Carbon Nanotubes. *J. Mater. Chem.* **2011**, *21*, 171–180.
45. Ma, Y. D.; Dai, Y.; Guo, M.; Niu, C. W.; Zhu, Y. T.; Huang, B. B. Evidence of the Existence of Magnetism in Pristine VX_2 Monolayers (X = S, Se) and Their Strain-Induced Tunable Magnetic Properties. *ACS Nano* **2012**, *6*, 1695–1701.
46. Yang, X. P.; Wu, G. Itinerant Flat-Band Magnetism in Hydrogenated Carbon Nanotubes. *ACS Nano* **2009**, *3*, 1646–1650.
47. Gorria, P.; Martínez-Blanco, D.; Blanco, J. A.; Pérez, M. J.; Hernando, A.; Barquín, L. F.; Smith, R. I. High-Temperature Induced Ferromagnetism on γ-Fe Precipitates in FeCu Solid Solutions. *Phys. Rev. B* **2005**, *72*, 014401.
48. Liu, F.; Ming, P. B.; Li, J. *Ab Initio* Calculation of Ideal Strength and Phonon Instability of Graphene Under Tension. *Phys. Rev. B* **2007**, *76*, 064120.
49. Lee, C. G.; Wei, X. D.; Kysar, J. W.; Hone, J. Measurement of the Elastic Properties and Intrinsic Strength of Monolayer Graphene. *Science* **2008**, *321*, 385–388.
50. Kou, L.; Tang, C.; Guo, W.; Chen, C. Tunable Magnetism in Strained Graphene with Topological Line Defect. *ACS Nano* **2011**, *5*, 1012–1017.
51. Ma, Y.; Dai, Y.; Guo, M.; Niu, C.; Yu, L.; Huang, B. Strain-Induced Magnetic Transitions in Half-Fluorinated Single Layers of BN, GaN and Graphene. *Nanoscale* **2011**, *3*, 2301–2306.
52. Wang, Y.; Yang, R.; Shi, Z.; Zhang, L.; Shi, D.; Wang, E.; Zhang, G. Super-Elastic Graphene Ripples for Flexible Strain Sensors. *ACS Nano* **2011**, *5*, 3645–3650.
53. Young, R. J.; Gong, L.; Kinloch, I. A.; Riaz, I.; Jalil, R.; Novoselov, K. S. Strain Mapping in a Graphene Monolayer Nanocomposite. *ACS Nano* **2011**, *5*, 3079–3084.
54. Frank, O.; Tsoukleri, G.; Parthenios, J.; Papagelis, K.; Riaz, I.; Jalil, R.; Novoselov, K. S.; Galiotis, C. Compression Behavior of Single-Layer Graphenes. *ACS Nano* **2010**, *4*, 3131–3138.
55. Wang, Z. G.; Zu, X. T.; Gao, F.; Weber, W. J. Atomistic Simulations of The Mechanical Properties of Silicon Carbide Nanowires. *Phys. Rev. B* **2008**, *77*, 224113.
56. Wang, Z. G.; Zu, X. T.; Yang, L.; Gao, F.; Weber, W. J. Atomistic Simulations of the Size, Orientation, and Temperature Dependence of Tensile Behavior in GaN Nanowires. *Phys. Rev. B* **2007**, *76*, 045310.
57. Yu, S.; Zheng, W.; Wang, C.; Jiang, Q. Nitrogen/Boron Doping Position Dependence of The Electronic Properties of a Triangular Graphene. *ACS Nano* **2010**, *4*, 7619–7629.
58. Li, L.; Qin, R.; Li, H.; Yu, L.; Liu, Q.; Luo, G.; Gao, Z.; Lu, J. Functionalized Graphene for High-Performance Two-Dimensional Spintronics Devices. *ACS Nano* **2011**, *5*, 2601–2610.
59. Zeng, M.; Feng, Y.; Liang, G. Graphene-Based Spin Caloritronics. *Nano Lett.* **2011**, *11*, 1369–1373.
60. Maassen, J.; Ji, W.; Guo, H. Graphene Spintronics: The Role of Ferromagnetic Electrodes. *Nano Lett.* **2010**, *11*, 151–155.
61. Cantele, G.; Lee, Y.-S.; Ninno, D.; Marzari, N. Spin Channels in Functionalized Graphene Nanoribbons. *Nano Lett.* **2009**, *9*, 3425–3429.
62. Wang, Y.; Huang, Y.; Song, Y.; Zhang, X.; Ma, Y.; Liang, J.; Chen, Y. Room-Temperature Ferromagnetism of Graphene. *Nano Lett.* **2008**, *9*, 220–224.
63. Herwadkar, A.; Lambrecht, W. R. L. Mn-Doped ScN: A Dilute Ferromagnetic Semiconductor with Local Exchange Coupling. *Phys. Rev. B* **2005**, *72*, 235207.
64. Jin, H.; Dai, Y.; Huang, B. B.; Whangbo, M. H. Ferromagnetism of Undoped GaN Mediated by Through-Bond Spin Polarization Between Nitrogen Dangling Bonds. *Appl. Phys. Lett.* **2009**, *94*, 162505.
65. Gorria, P.; Martinez-Blanco, D.; Perez, M. J.; Blanco, J. A.; Hernando, A.; Laguna-Marco, M. A.; Haskel, D.; Souza-Neto, N.; Smith, R. I.; Marshall, W. G.; *et al*. Stress-Induced Large Curie Temperature Enhancement in Fe(64)Ni(36) Invar Alloy. *Phys. Rev. B* **2009**, *80*, 064421.